

RESEARCH

Open Access



# An in-vivo comparison of stimulated-echo and motion compensated spin-echo sequences for 3 T diffusion tensor cardiovascular magnetic resonance at multiple cardiac phases

Andrew D. Scott<sup>1,2\*</sup>, Sonia NIELLES-Vallespin<sup>2,3</sup>, Pedro F. Ferreira<sup>1,2</sup>, Zohya Khalique<sup>1</sup>, Peter D. Gatehouse<sup>1,2</sup>, Philip Kilner<sup>1,2</sup>, Dudley J. Pennell<sup>1,2</sup> and David N. Firmin<sup>1,2</sup>

## Abstract

**Background:** Stimulated-echo (STEAM) and, more recently, motion-compensated spin-echo (M2-SE) techniques have been used for in-vivo diffusion tensor cardiovascular magnetic resonance (DT-CMR) assessment of cardiac microstructure. The two techniques differ in the length scales of diffusion interrogated, their signal-to-noise ratio efficiency and sensitivity to both motion and strain. Previous comparisons of the techniques have used high performance gradients at 1.5 T in a single cardiac phase. However, recent work using STEAM has demonstrated novel findings of microscopic dysfunction in cardiomyopathy patients, when DT-CMR was performed at multiple cardiac phases. We compare STEAM and M2-SE using a clinical 3 T scanner in three potentially clinically interesting cardiac phases.

**Methods:** Breath hold mid-ventricular short-axis DT-CMR was performed in 15 subjects using M2-SE and STEAM at end-systole, systolic sweet-spot and diastasis. Success was defined by  $\geq 50\%$  of the myocardium demonstrating normal helix angles. From successful acquisitions DT-CMR results relating to tensor orientation, size and shape were compared between sequences and cardiac phases using non-parametric statistics. Strain information was obtained using cine spiral displacement encoding with stimulated echoes for comparison with DT-CMR results.

**Results:** Acquisitions were successful in 98% of STEAM and 76% of M2-SE cases and visual helix angle (HA) map scores were higher for STEAM at the sweet-spot and diastasis. There were significant differences between sequences ( $p < 0.05$ ) in mean diffusivity (MD), fractional anisotropy (FA), tensor mode, transmural HA gradient and absolute second eigenvector angle (E2A). Differences in E2A between systole and diastole correlated with peak radial strain for both sequences ( $p \leq 0.01$ ).

**Conclusion:** M2-SE and STEAM can be performed equally well at peak systole at 3 T using standard gradients, but at the sweet-spot and diastole STEAM is more reliable and image quality scores are higher. Differences in DT-CMR results are potentially due to differences in motion sensitivity and the longer diffusion time of STEAM, although the latter appears to be the dominant factor. The benefits of both sequences should be considered when planning future studies and sequence and cardiac phase specific normal ranges should be used for comparison.

**Keywords:** Diffusion, Diffusion tensor imaging, Cardiac, Heart, STEAM, Spin-echo, Motion compensation

\* Correspondence: a.scott@rbht.nhs.uk

<sup>1</sup>Cardiovascular Magnetic Resonance Unit, Royal Brompton and Harefield NHS Foundation Trust and Imperial College London, Sydney Street, London, UK

<sup>2</sup>National Heart and Lung Institute, Imperial College London, Sydney Street, London, UK

Full list of author information is available at the end of the article



## Background

There is a growing interest in diffusion tensor cardiovascular magnetic resonance (DT-CMR) due to its unique ability to noninvasively interrogate the myocardial microstructure, and recent publications have demonstrated potential clinical applications [1–7]. However, the dynamic nature of the heart makes it a challenging target for DT-CMR. Initial in-vivo DT-CMR studies used a stimulated echo acquisition mode (STEAM) based echo-planar imaging (EPI) technique, with diffusion encoding gradients at identical trigger times in two successive cardiac cycles [8, 9]. Diffusion is encoded over one complete cardiac cycle (the diffusion time,  $\Delta$ ) and relatively large diffusion weightings (b-values) can be achieved with relatively small gradient pulses. This allows STEAM DT-CMR to be performed at time points throughout the cardiac cycle [6, 10], which has been used to demonstrate impairment of the rotation of the aggregates of cardiomyocytes known as sheetlets in hypertrophic and dilated cardiomyopathy patients [6, 7, 11]. A recent validation study [6] demonstrated excellent similarity between angular DT-CMR measures obtained in hearts imaged while beating and arrested in-vivo, ex-vivo and histologically in relaxed and contracted states. However, differences in myocardial position and conformation between the diffusion encoding gradients result in changes in image phase and signal intensity. This makes studies difficult during arrhythmia or during free-breathing [9]. The measured diffusion is also affected by the strain history of the myocardium between the encoding gradients [12] although the size of this effect is under debate [1, 6, 13].

To deal with the effects of strain on the diffusion tensor a correction model has been used with input from 3D strain data [12]. Alternatively, using the same model, times in the cardiac cycle where strain has no effect (so called strain “sweet-spots”) on measured diffusion can be identified from strain data [14]. These techniques also require a measurement of 3D strain throughout the cardiac cycle.

Another approach is to use a spin-echo (SE) sequence similar to neurological diffusion tensor techniques [15, 16]. The duration of the diffusion gradients when using SE sequences is usually too long to identify a matching quiescent cardiac phase, but motion compensation may be incorporated into the diffusion encoding gradients [17]. Recently, velocity and acceleration compensated (M2) [18, 19] gradients have been used to perform SE DT-CMR in vivo [20, 21]. A comparison between STEAM and M2-SE techniques [21] described improved SNR efficiency and a more linear transmural distribution of helix angles using M2-SE, as well as differences in fractional anisotropy (FA) and mean diffusivity (MD) between sequences. The short diffusion time of M2-SE techniques means that the technique does not require two cardiac cycles per image, strain effects are minimised and the 50% signal loss inherent to stimulated echoes is avoided. The long diffusion encoding

gradient pulses for M2-SE avoid the T1 signal loss during the time between the second and third radiofrequency (RF) pulses (the mixing time) but result in long echo times (TE) and consequential signal loss. However, previously published in-vivo human demonstrations of M2-SE DT-CMR have predominantly used high performance gradient systems at 1.5 T [20, 21].

In this work we implement an M2-SE DT-CMR sequence on a 3 T clinical CMR scanner with standard gradients and directly compare to the STEAM sequence using matched protocols at three cardiac phases. We also consider the contribution of strain to the differences in DT-CMR results between the cardiac phases and sequences.

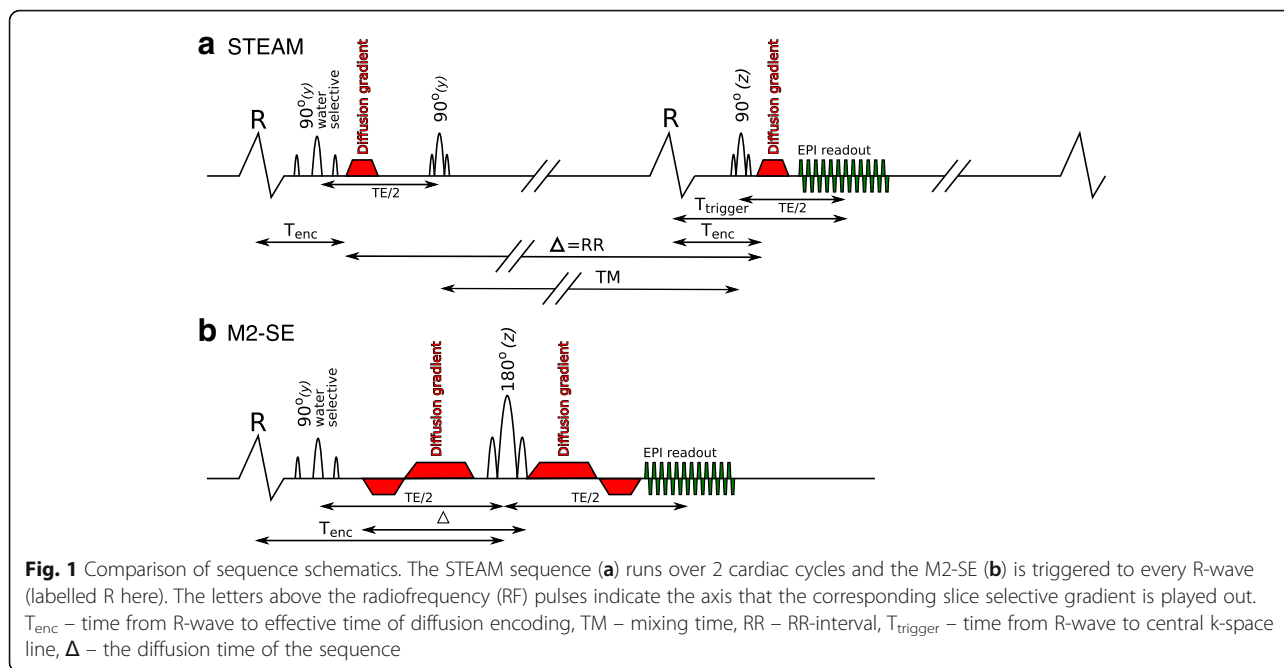
## Methods

Fifteen healthy subjects (9 male, median age 24, range 20–36) were recruited with consent according to ethical approval. Images were acquired using a Siemens 3 T scanner (Skyra, Siemens Healthineers, Erlangen, Germany) with standard gradients ( $43\text{mT}\cdot\text{m}^{-1}$  and  $180\text{T}\cdot[\text{m}\cdot\text{s}]^{-1}$  per axis) using anterior (18-elements) and posterior (8–12 elements) RF coils. Balanced steady-state free-precession cine imaging was used to identify a mid-ventricular short-axis plane and the end-systolic and end-diastolic periods for subsequent acquisitions.

### DT-CMR sequences

The STEAM EPI DT-CMR sequence was described in previous work [9] (Fig. 1a). A breath-hold SE EPI DT-CMR sequence was implemented with first and second order motion compensated diffusion encoding gradients (M2-SE) to minimise signal loss artefacts caused by constant velocity and acceleration during the gradients (Fig. 1b). The gradient design was based on that described by Welsh et al. [18] and Stoeck et al. [20].

To facilitate comparisons, imaging parameters were matched between sequences. For both sequences, EPI readout duration was reduced by a “zone-selected” technique [22]. A sensitivity encoding (SENSE) [23] acceleration factor of 2 was used to further reduce the EPI readout length. No partial Fourier sampling was used. Identical EPI readouts were used for both sequences, with a 13 ms duration, 2442 Hz/pixel bandwidth and 0.51 ms echo spacing. Spatial resolution was  $2.8 \times 2.8\text{mm}^2$ ,  $1.4 \times 1.4\text{mm}^2$  via zero-filled reconstruction and 8 mm slice thickness. Investigation of the sequence used in a previous comparison [24] demonstrated a mismatch in the effective slice thickness between the techniques. For this comparison, sinc shaped pulses were used for the final RF pulse in both sequences and the full-width half-maximum of the slice profile was adjusted to 8 mm. The M2-SE sequence acquires one spin-echo every cardiac cycle (RR-interval), whereas STEAM acquires a stimulated echo every other cardiac cycle. In each breath-hold the first spin or stimulated echo is used for EPI phase correction lines and the second for parallel



imaging references data. Then, the “b0” image is acquired (where diffusion encoding is replaced with spoiler gradients;  $b = 34s \cdot mm^{-2}$  for STEAM and  $b = 30s \cdot mm^{-2}$  for M2-SE), followed by each of the 6 diffusion encoding directions used (7 or 14 RR intervals for M2-SE or STEAM respectively). In order to produce similar breath-hold durations, two averages per breath-hold were acquired for M2-SE (total 16RR-intervals vs. 18RR-intervals for STEAM). Based on previous M2-SE studies  $b_{main} = 450s \cdot mm^{-2}$  was used for both sequences. The total durations were 2.4 ms for each of the STEAM diffusion encoding gradients and 9.1 and 17.5 ms for each of the short and long M2-SE diffusion encoding gradients. Rather than using “b0” images in the tensor calculation, additional data was acquired for use as the reference with  $b_{ref} = 150s \cdot mm^{-2}$  in the same 6 directions as the  $b_{main}$  data [20, 25]. For STEAM 8 averages and for M2-SE 16 averages (8 breath holds) were used for  $b_{main}$  and 1 (STEAM) or 2 (M2-SE) averages (1 breath-hold) were used for  $b_{ref}$ . Acquisition was triggered to alternate R-waves ( $TR = 2$  RR-intervals) for STEAM and every R-wave for M2-SE ( $TR = 1$  RR-interval). A 1–2–1 binomial water excitation RF pulse was used for the initial excitation in both sequences. Flip angles were  $90^\circ$  in the STEAM sequence and  $90^\circ - 180^\circ$  in the M2-SE sequence. TE was 25 ms for STEAM and 76 ms for M2-SE.

**Phantom signal to noise ratio measurements**

Signal-to-noise ratio (SNR) was compared between the sequences using a cylindrical agar phantom (13 cm diameter,  $40g \cdot L^{-1}$  agar in tap water). Transverse images were acquired (50 averages) with the phantom axis aligned with

the magnetic field. Imaging parameters are as described above with a simulated RR-interval of 1000 ms. The “b0” images ( $b_{ref} = 34s \cdot mm^{-2}$ , STEAM and  $b_{ref} = 30s \cdot mm^{-2}$ , M2-SE) were compared. Pixelwise SNR per image was calculated as the ratio of the mean to standard deviation of the signal in each pixel over time [26] and the mean value was taken from a region of interest (ROI) drawn in the centre of the phantom. Adapting the theory described by von Deuster et al. [21] (who compared SNR efficiency), the ratio of the mean SNR per image in the phantom was compared to the theoretical value calculated via:

$$\frac{SNR_{SE}}{SNR_{STEAM}} = \frac{\left(1 - e^{-\frac{Trecov_{SE}}{T_1}}\right) \cdot e^{-\frac{TE_{SE}}{T_2}} \cdot e^{-b_{SE} \cdot D}}{\frac{1}{2} \left(1 - e^{-\frac{Trecov_{STEAM}}{T_1}}\right) \cdot e^{-\frac{TE_{STEAM}}{T_2}} \cdot e^{-b_{STEAM} \cdot D} \cdot e^{-\frac{TM}{T_1}}} \tag{1}$$

where  $Trecov_{SE}$  and  $Trecov_{STEAM}$  are the inter-shot longitudinal recovery times for the M2-SE and STEAM sequences respectively (1RR interval in both cases),  $TE_{SE}$  and  $TE_{STEAM}$  are TE for each of the sequences,  $D$  is the diffusivity of the agar phantom,  $b_{SE}$  and  $b_{STEAM}$  are the b-values for each of the sequences and  $TM$  is the mixing time of the STEAM sequence (1 RR-interval). A flip angle of  $90^\circ$  was assumed for each of the STEAM RF pulses and  $90^\circ - 180^\circ$  for the pulses in the M2-SE sequence.

**In-vivo imaging**

DT-CMR was performed at systole, diastole and the systolic sweet-spot using both STEAM and M2-SE. For the M2-SE sequence, systolic acquisitions were timed to acquire the centre of k-space at end systole and diastolic

acquisitions were timed to place diffusion encoding gradients and image data acquisition during the most stationary period of diastole (assessed visually on cine images). Where images from the first M2-SE breath-hold were poor quality in systole or diastole, the acquisition was optimised by repetition at trigger delays  $\pm 20$  ms. STEAM data for the systolic or diastolic timing were acquired immediately after the corresponding M2-SE acquisition and trigger times were set to match the timing of the centre of the diffusion encoding gradients between sequences. Based on our previous work [27] and the mean sweet-spot timing used in [21] of 142 ms we used a fixed time of 150 ms from the R-wave to the centre of the diffusion encoding for sweet-spot imaging. While the M2-SE acquisition timing was optimised and data was acquired before the STEAM data at each cardiac phase, the order in which the cardiac phases were acquired was randomised between subjects.

### Strain

Breath-hold spiral cine displacement encoding with stimulated echoes (DENSE) [28, 29] was performed with a novel sequence accelerated by using a reduced field of view in two dimensions [30]. 2D acquisitions with 2-direction encoding were performed in the same plane as the DT-CMR acquisitions at a  $3.3 \times 3.3 \text{ mm}^2$  spatial resolution, 30 ms temporal resolution, 8 mm slice thickness,  $224 \times 224 \text{ mm}^2$  field of view and 14 RR-interval breath holds. A variable flip angle with a maximum of  $20^\circ$  was used, chemical shift selective fat saturation, TE = 1 ms, TR = 15 ms, 2 spiral interleaves per temporal frame, 6 ms per spiral and 4 interleaves per image. Displacement encoding frequency was  $0.06 \text{ cycles} \cdot \text{mm}^{-1}$  and artefacts from unwanted echo pathways were minimised using CSPAMM-like encoding and through-plane spoiling ( $0.08 \text{ cycles} \cdot \text{mm}^{-1}$ ) [31].

### Processing

DT-CMR data was processed using in-house MATLAB (Mathworks, Natick, Massachusetts, USA) software as described in previous work [1, 25, 32, 33]. The  $b_{\text{ref}}$  ( $150 \text{ s} \cdot \text{mm}^{-2}$ ) and  $b_{\text{main}}$  ( $450 \text{ s} \cdot \text{mm}^{-2}$ ) images were used to calculate the diffusion tensor. Frames corrupted by motion were discarded after visual assessment and the images were registered using a rigid translation. A variable amount of myocardial blood signal was present in the M2-SE images. Pixels containing blood with a very high signal intensity were nulled based on their intensity prior to the image registration step and the original signal intensities were returned after registration. A diffusion tensor was calculated at every pixel from the registered magnitude images using a linear least squares inversion. Each image was included separately within the matrix inversion without averaging and for the STEAM sequence the b-values were corrected for the RR-interval on a beat-to-beat basis.

Pixel-wise maps of helical angle (HA), absolute value of the second eigenvector angle (E2A) [1], fractional anisotropy (FA), tensor mode (mode) [34], mean diffusivity (MD) and each of the three eigenvalues (E1, E2, E3) were calculated. SNR per image was calculated in an ROI in the septal mesocardium (away from blood signal and artefacts) in the “b0” images ( $b = 34 \text{ s} \cdot \text{mm}^{-2}$  for STEAM [9 images] and  $b = 30 \text{ s} \cdot \text{mm}^{-2}$  for M2-SE [18 images]) without averaging using the repeated measurement technique [9, 26]. To facilitate quantitative comparisons of HA, wall thickness normalised helical angle gradient (HAG) in units of  $^\circ/\%$  was calculated from epi- to endocardium radial profiles [35, 36]. For comparative analysis, mean left ventricular (LV) values for all parameters except E2A were calculated after removing papillary muscles and the right ventricular portion of the septum. Median LV E2A values were used because E2A is not expected to be normally distributed.

DT-CMR data quality was assessed by scoring the HA maps on the assumption of a circumferential linear variation of HA from epi- to endocardium. A score of 3 was given to HA maps with visually  $>95\%$  normal transmural HA variation, 2 for  $>75\%$ , 1 for  $>50\%$  and 0 for  $<50\%$ . Acquisitions with scores of 0 were considered a failure and excluded from further analysis. Scoring was performed separately in a randomised order by two blinded observers (4 and 2 years of DT-CMR experience) and conflicts were resolved by consensus. Based on the assumption of a constant transverse angle within each slice and a linear transmural HA profile, the standard deviation of the transverse angle [21] (TA std) and both the Pearson  $R^2$  and root mean squared error of the linear regression of the transmural HA profiles (HA  $R^2$  and HA RMSE) were used as quantitative DT-CMR quality measures.

Global peak radial and circumferential LV strains were calculated from the cine spiral DENSE data using DENSE Analysis software [37, 38]. We compared peak strains with the differences in diffusion derived parameters (E2A, HAG, MD, FA and mode) between systole and diastole, and between the sequences at each cardiac phase.

### Statistical analysis

All statistics were calculated in MATLAB (Mathworks). Global LV DT-CMR results were compared using a Wilcoxon test between sequences at systole, sweet-spot and diastole. Results were compared between cardiac phases using Friedman test with Bonferroni corrected Wilcoxon pairwise comparisons. Differences between DT-CMR results in systole and diastole and between techniques were correlated with peak radial and circumferential strains (Pearson correlation coefficient).  $P < 0.05$  was considered significant.

## Results

### Phantom study

The phantom was found to have a T1 = 1090 ms (modified Look-Locker imaging, 5(3)3 [39, 40]) and T2 = 51 ms



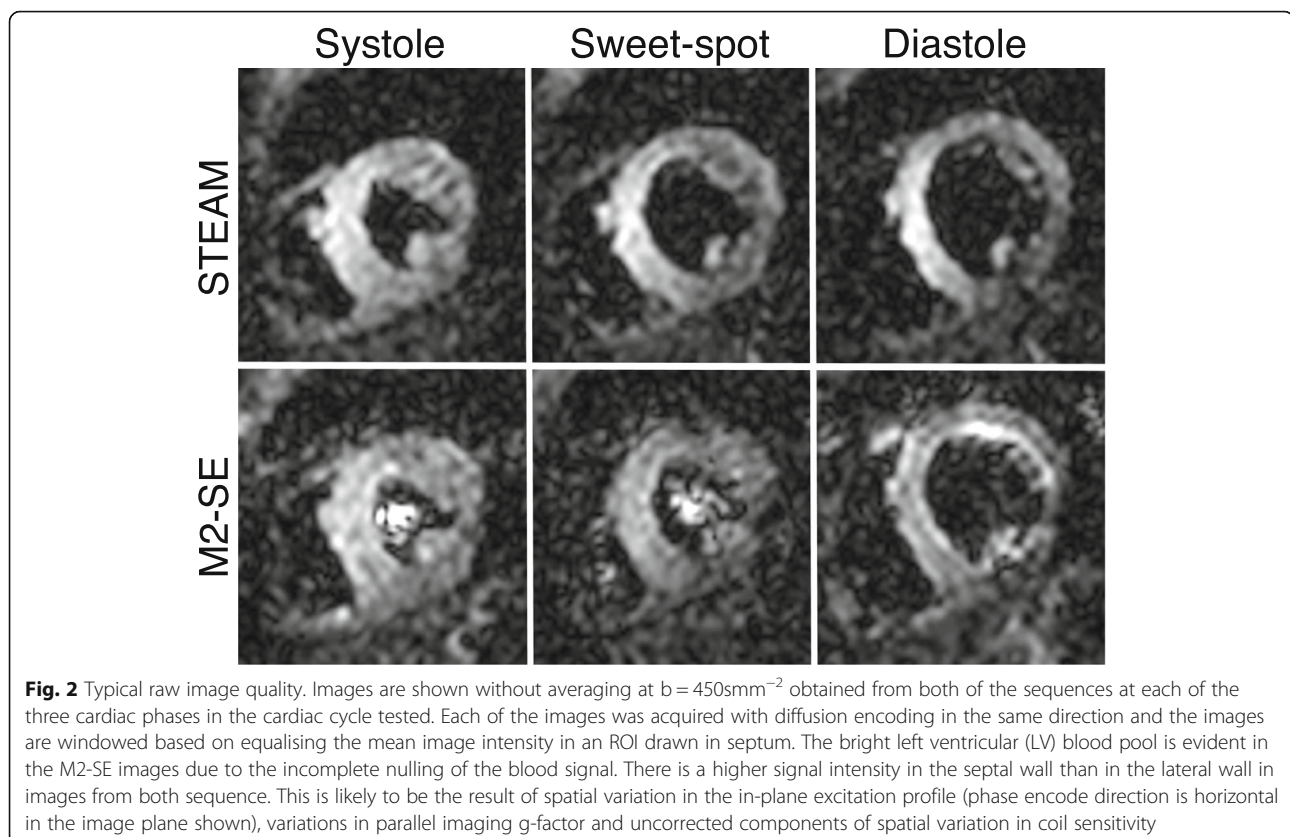
(repeated spin-echo acquisitions with increasing TE) and a mean diffusivity of  $1.2 \times 10^{-3} \text{mm}^2 \cdot \text{s}^{-1}$  (product Stejskal-Tanner spin-echo EPI sequence). The resulting theoretical SNR ratio (M2-SE/STEAM) was 1.85 and the measured value (mean  $\pm$  standard deviation within an ROI) was  $1.75 \pm 1.14$ .

### In-vivo imaging

DT-CMR studies were of a sufficient quality for further analysis in 44/45 STEAM studies (1 diastolic acquisition scored 0) and in 34/45 M2-SE studies (14/15 systolic, 12/15 sweet-spot, and 8/15 diastolic). Figure 2 shows the typical image quality for raw unaveraged images. Examples of good quality DT-CMR parameter maps are shown in Fig. 3. For contrast, a diastolic example where STEAM was successful (scored 3), but M2-SE was of poor quality (scored 0) is shown in Fig. 4 (with corresponding raw images shown in Additional file 1: Figure S1 and S2). The median image quality at each cardiac phase was (STEAM/M2-SE): 3/3 for systole, 3/2 for sweet-spot, 2/1 for diastole. Histograms of the image quality scores are shown in Fig. 5 and scores were significantly different between the sequences at the sweet-spot and in diastole ( $p < 0.01$ ). Mean  $\pm$  standard deviation RR-interval was  $970 \pm 140$  ms. There was a significant correlation (Spearman) between the image quality score and the RR-interval for the STEAM data at the sweet spot ( $\text{Rho} = 0.58$ ,  $p = 0.02$ ) and for M2-SE data in diastole ( $\text{Rho}$

$= 0.73$ ,  $p = 0.002$ ), see Additional file 1: Figure S3. Correlations between mean RR-interval and image quality score were not significant for other combinations of sequence and cardiac phase or between image score and the intra-subject RR-interval variability (standard deviation).

Global LV values of MD and FA are shown in fig. 6 and both HAG and E2A are plotted in fig. 7. Global tensor mode is plotted in Additional file 1: Figure S4; TA std., HA  $R^2$  and HA RMSE in SAdditional file 1: Figure S5; and SNR per image in a mesocardial septal ROI and mean signal in the same ROI are plotted in Supporting Fig. S6. The statistics shown in the figures provide a comparison between sequences at each cardiac phase while Supporting Table S1 compares the cardiac phases for each sequence. Additional file 1: Table S1 includes E2A measures obtained using both the median and mean over the LV to allow for comparison with previous work [1, 30, 31]. There are significant differences ( $p < 0.05$ ) between the two sequences at all three cardiac phases for MD, FA, tensor mode, HAG and E2A. The non-subjective data quality measures were suggestive of better quality STEAM data at the sweet-spot (TA std. and HA RMSE significantly lower and HA  $R^2$  significantly higher,  $p < 0.05$ ) and TA std. was suggestive of better quality diastolic STEAM data ( $p < 0.05$ ). SNR per image was significantly higher at all three cardiac phases for STEAM ( $p < 0.01$ ), but there



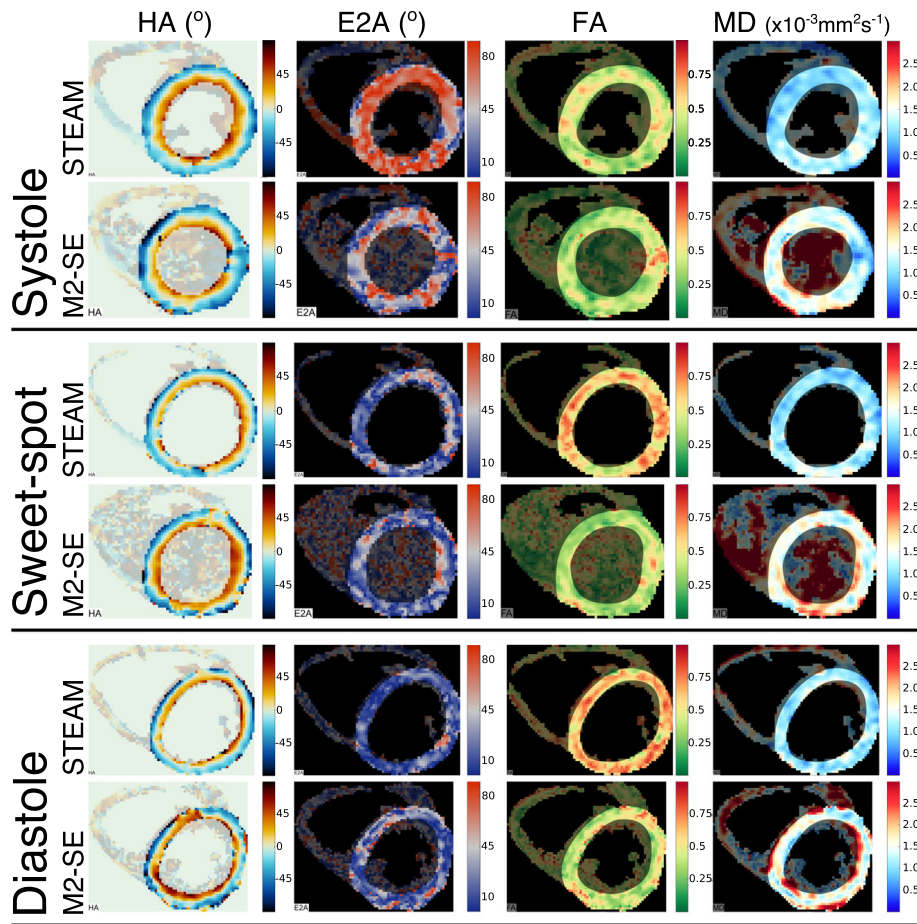


**Fig. 3** Example of successful DT-CMR maps. Results are shown from both sequences at all three cardiac phases from a subject where image quality was good in all acquisitions. The parameter maps are masked to indicate the region of the LV used in the analysis

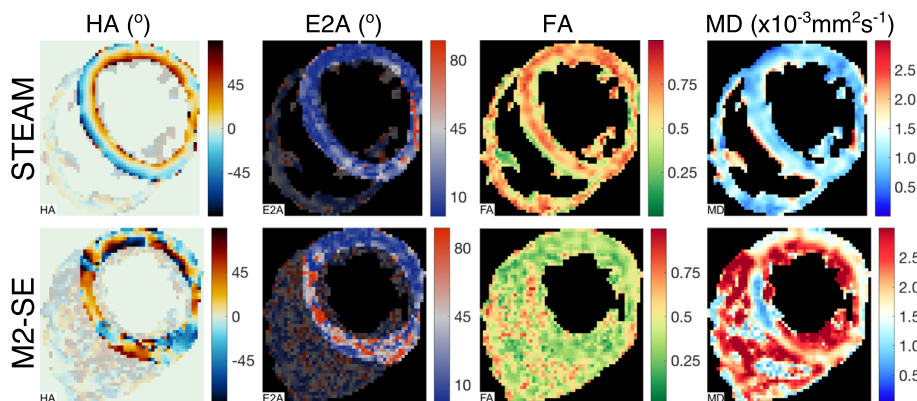
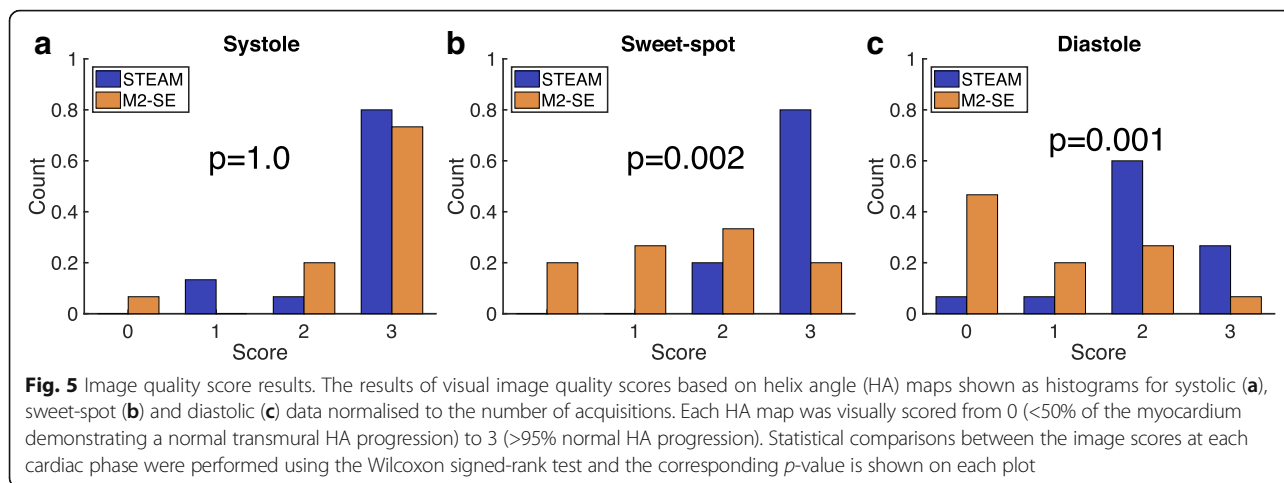


**Fig. 4** Example of unsuccessful M2-SE DT-CMR parameter maps. Maps are shown from a subject where M2-SE imaging was unsuccessful in diastole (scored 0), but diastolic STEAM imaging in the same subject scored 3. The raw images for these two datasets are provided in Supplementary Fig. S1 and S2 for the STEAM and M2-SE acquisitions respectively



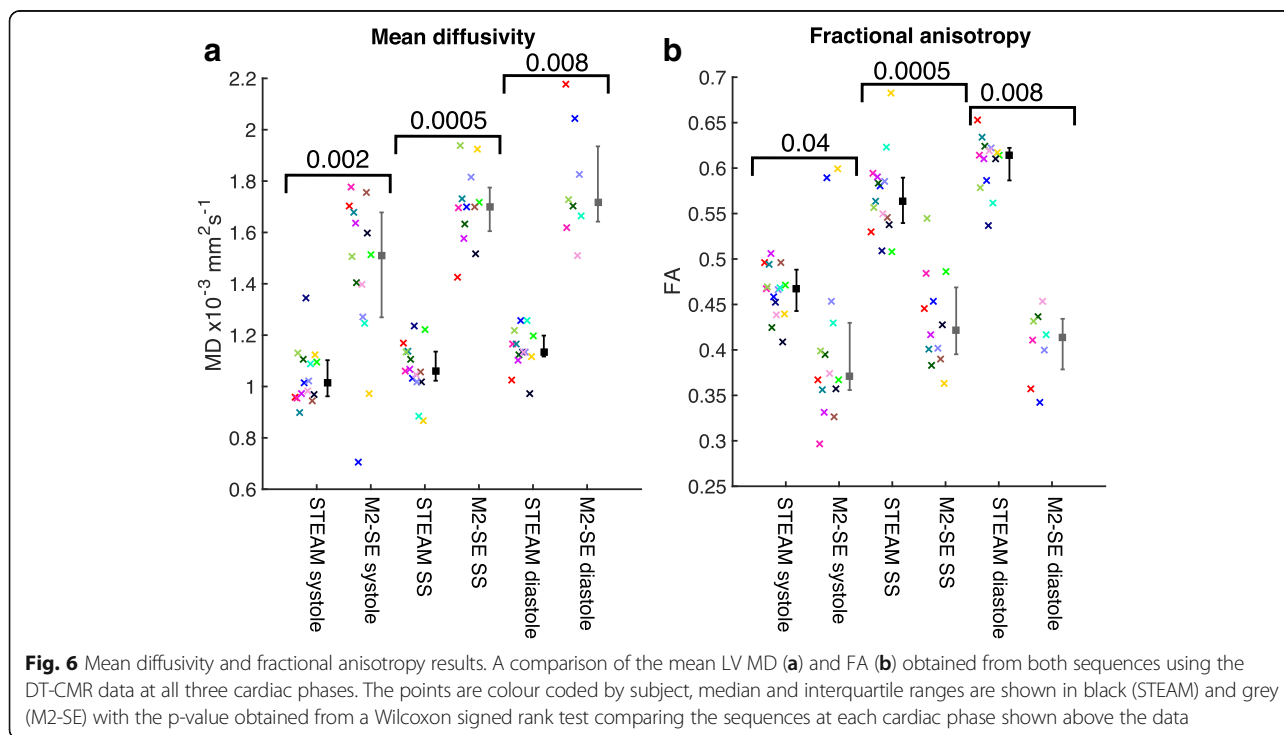
were no significant differences between sequences in the mean signal. For the STEAM acquisitions there were significant differences ( $p < 0.05$  or  $p < 0.017$  after Bonferroni correction) between all three cardiac phases for E2A and E1; between systole and both sweet-spot and diastole for FA and E3; between diastole and both sweet-spot and systole for HA  $R^2$  and HAG; between systole and diastole for MD; and between systole and both sweet-spot and diastole for TA std. For the M2-SE acquisitions there were significant differences between cardiac phases only for SNR per image.

The increased MD and reduced FA using the M2-SE sequence is reflected in the larger eigenvalues with smaller relative differences between them when compared to the STEAM results. In general, the eigenvalue

histograms in Fig. 8 show less variation between subjects using the STEAM sequence than M2-SE and the average histograms for M2-SE have a broader peak as a result. The upper tail of the primary eigenvalue histogram for the STEAM sequence extends to around  $3 \times 10^{-3} \text{mm}^2 \cdot \text{s}^{-1}$ , which is the diffusivity of free water at 37 °C [41]. In contrast, the tail of the primary eigenvector distribution extends to around  $5 \times 10^{-3} \text{mm}^2 \cdot \text{s}^{-1}$  for the M2-SE sequence.

The tensor differences between the two sequences are also reflected in the systolic superquadric glyph representation of the diffusion tensor shown in Fig. 9.

The median [interquartile range] peak strains were 0.50 [0.15] and  $-0.177$  [0.016] in the radial and circumferential



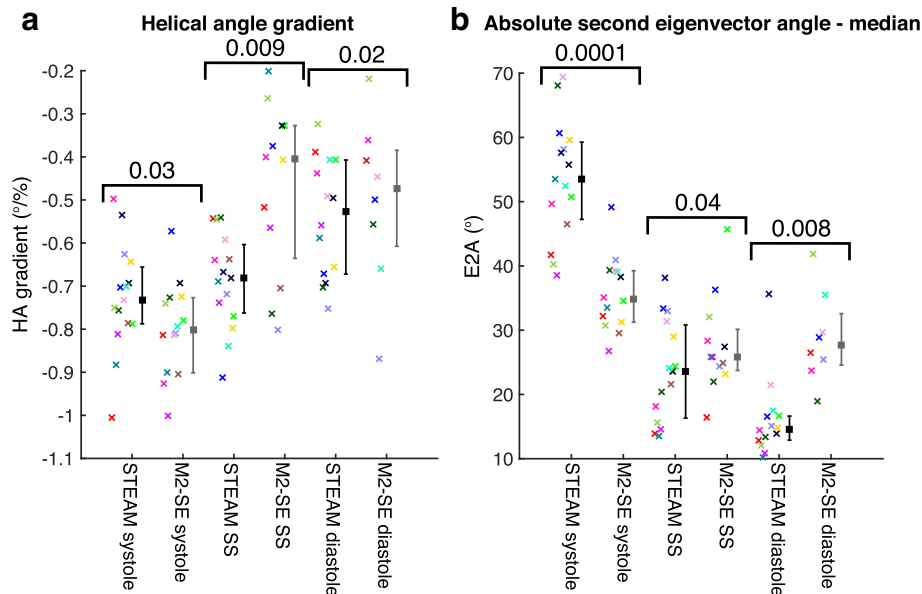


**Fig. 7** Helix angle gradient and E2A results. A comparison of the mean LV helical angle gradient (HAG) (a) and second eigenvector angle (E2A) (b) obtained from both sequences using the DT-CMR data at all three cardiac phases in the cardiac cycle. The points are colour coded by subject, median and interquartile ranges are shown in black (STEAM) and grey (M2-SE) with the p-value obtained from a Wilcoxon signed rank test comparing the sequences at each cardiac phase shown above the data

directions respectively. Additional file 1: Table S2 lists all the correlations with  $p < 0.05$  obtained when comparing the differences in DT-CMR results (systole – diastole and STEAM – M2-SE) with peak radial and circumferential strains and the corresponding plots are shown in Fig. 10. No significant correlations were found when comparing the sequence or cardiac phase differences with peak circumferential strain. Using STEAM, the difference in both FA and E2A between systole and diastole significantly correlates with peak radial strain ( $p = 0.05$  and  $p = 0.003$  respectively). Using M2-SE, the significant correlation between E2A difference and peak radial strain is still present ( $p = 0.01$ ). The E2A difference between the two sequences also correlates with peak radial strain in both systole and diastole ( $p < 0.01$ ).

**Discussion**

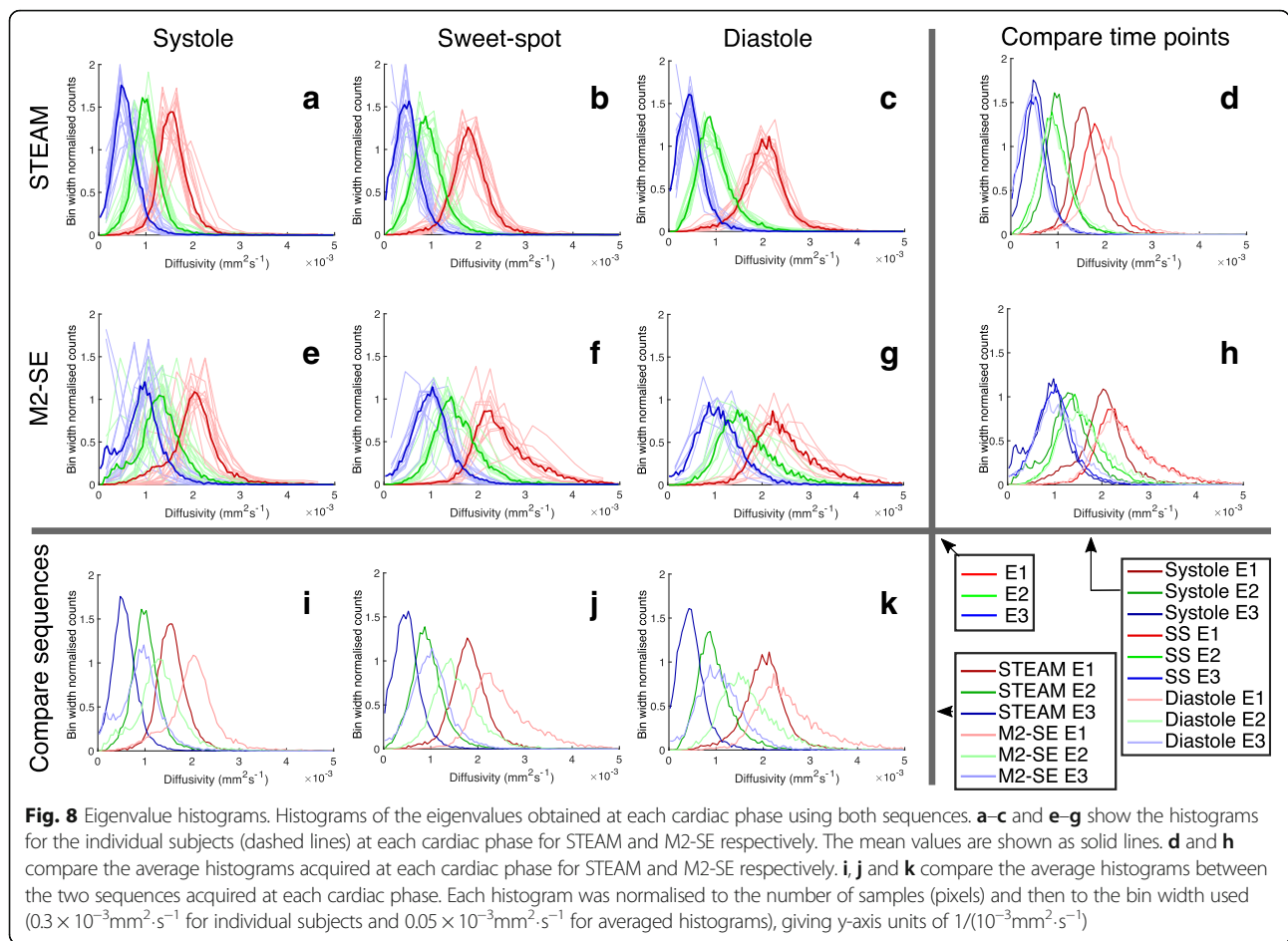
In this work we have implemented a 1st and 2nd order motion compensated (M2) SE DT-CMR sequence and compared results to those obtained from a monopolar STEAM sequence at 3 points in the cardiac cycle. To the best of our knowledge, this is the first published work to compare these sequences at multiple points in the cardiac cycle. While standard performance gradients have been used for velocity and acceleration compensated (M2) diffusion prepared techniques at 3 T [5, 19] and M2-SE has been demonstrated with a range of gradients strengths at 1.5 T during systolic contraction [20, 21, 42], this is the first study to demonstrate M2-SE with standard

performance gradients at 3 T. While we were able to perform both sequences at all cardiac phases in most subjects, there were clear differences in reliability, image quality and the DT-CMR results.

For the healthy cohort in this work, the sequences performed similarly in systole, but STEAM was more reliable and image quality scores and quantitative measures were suggestive of better quality data in the sweet spot and diastole. A substantial number of M2-SE acquisitions were deemed to have failed (7/15 in diastole). In contrast, STEAM was successful in all but 1 acquisition and the visual image quality scores were significantly higher for the STEAM sequence at the sweet-spot ( $p = 0.002$ ) and diastole ( $p = 0.001$ ).

There are differences between the values of DT-CMR results the two sequences provide. Significant differences were present in FA, MD, tensor mode, E2A and HAG at all three cardiac phases (all  $p < 0.05$ ). This is to be expected given the differences between the two approaches. The longer TE of M2-SE (76 ms vs. 25 ms STEAM) results in greater T2 weighting of the images. The reference and diffusion-weighted images used to calculate the diffusion tensor use the same TE and, therefore cancel the effects of T2 weighting on the diffusivity calculation. However, tissue components with a shorter T2 value will contribute less to the measured signal (and therefore the calculated diffusion tensor) than components with longer T2 values, particularly in the M2-SE acquisition. The exact influence of T2 on measured diffusion will depend convolutedly on T2 values



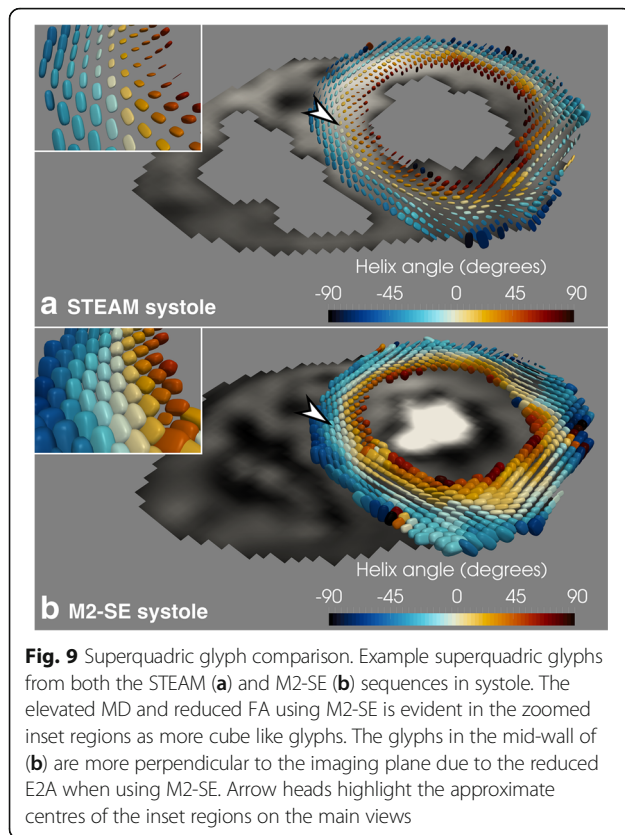


within the multiple tissue compartments and the trans-membrane water exchange rates between them. A similar multi-compartment problem also applies in regards to differences in the T1 weighting of the two sequences.

Another factor contributing to the differences in results is the differing sensitivity to cardiac motion of the two sequences. The STEAM sequence uses short diffusion encoding gradients, which minimises the detrimental effects of motion during the gradients (although inter-gradient motion is problematic). In contrast, the spin-echo sequence requires a much larger gradient area and the gradients are further extended in time in the M2-SE sequence in order to compensate for velocity and acceleration. While the M2 encoding gradients have a reduced sensitivity to motion, it requires that higher order motion components are minimal while they are run.

The higher failure rate of the M2-SE sequence at the sweet-spot and in diastasis could be attributed to uncompensated cardiac motion during the long diffusion encoding gradients, which is perhaps also consistent with the primary eigenvalues substantially exceeding that of free water in some pixels when using this sequence (Fig. 8). The largest number of studies failed in diastole

(7/15) and the diastolic M2-SE image quality score significantly increased with lengthening RR-intervals. The magnitude of cardiac motion is low in diastasis, but the motion trajectories may be complex. Welsh et al. [18] considered the effects of velocity, acceleration and jerk compensation on diffusion encoding gradients and concluded that 2nd order compensation was sufficient in rats. However, the increasing gradient duration as the motion compensation order increases, also makes it increasingly likely that more complex motion will occur during them. Recent work demonstrated increased cardiac motion and eddy current related signal loss in M2-SE sequences than in STEAM sequences [43], although very little of the difference in MD between sequences could be attributed to this. High performance gradient systems, such as those now commercially available with maximum gradient strength of  $80 \text{mT} \cdot \text{m}^{-1}$  at slew rates of  $200 \text{T} \cdot [\text{m} \cdot \text{s}]^{-1}$  may partially address the residual motion sensitivity of M2-SE. Stoeck et al. [20] used a maximum gradient amplitude/slew rate of  $80 \text{mT} \cdot \text{m}^{-1} / 100 \text{T} \cdot [\text{m} \cdot \text{s}]^{-1}$  to reduce the total M2 diffusion encoding time to 50 ms, versus 62 ms achieved here ( $TE = 73 \text{ms}$  versus  $TE = 76 \text{ms}$  here). In a study of the sensitivity of



the M2-SE technique to gradient strength, 2/6 systolic acquisitions failed when maximum gradient strengths were only  $30\text{mT}\cdot\text{m}^{-1}$  [42]. In order to fully understand the effects of cardiac motion on the results and success rates of both sequences in various points throughout the cardiac cycle, future work should consider computational simulations, extending the work of Mekkaoui et al. [44]. One of the difficulties with such simulations is that they will require in-vivo measures of 3D motion trajectories covering the whole cardiac cycle, accurate to at least 3rd order motion (jerk). Myocardial phase velocity mapping, with 3-direction encoding and retrospective cardiac gating [45] may be suited to acquiring such data.

Investigations of the optimum timing of the M2-SE sequence [20, 46] have found that triggering between 15% and 77% of the time from the R-wave to peak-systole (during systolic contraction) resulted in an acceptable level of motion related signal loss (although time points beyond peak-systole were not analysed). In this work, we found the highest success rate when the centre of k-space was timed to peak systole, equivalent to triggering at 75% of peak systole ( $TE = 75\text{ ms}$ , time to peak systole 300 ms). In comparison to other work, we found lower success rates at the systolic sweet-spot, which we defined as a constant 150 ms from the R-wave based on previous work considering the predicted effects of strain on STEAM data [27]. However, the three M2-SE acquisitions which failed at the

sweet-spot correspond to subjects with the maximum (100 bpm) and minimum (50 and 55 bpm) mean heart rates, suggesting that a fixed trigger time may not be best suited for M2-SE imaging.

A further difficulty with acquiring M2-SE data in diastasis is that the longer acquisition window frequently caused the scanner to miss the next R-wave. Based on DICOM timestamp information we estimate the proportion of missed triggers as 7% for diastolic M2-SE and 0.1–0.6% in other acquisitions. These missed triggers extend breath-hold durations and perturb the longitudinal magnetisation's steady-state, which is likely to result in errors in the calculated diffusion tensor. In earlier pilot work [24], we achieved a higher success rate for M2-SE imaging in diastasis (15/20 acquisitions successful) by triggering M2-SE to alternate R-waves ( $TR = 2RR$ -intervals). Principal component analysis – temporal maximum intensity projection (PCA-TMIP) post-processing technique [47] and related methods [48] could potentially be combined with M2-SE sequences to palliate its motion sensitivity. Alternatively, pharmacological methods of increasing the length of diastasis may be useful [49].

The strain history of the imaged tissue during the diffusion time affects the measured diffusion [12] and the long diffusion time of STEAM means it is more affected than M2-SE. We found significant correlations between peak radial strain and the difference between systolic and diastolic FA and E2A using STEAM ( $p < 0.05$ ). We did not perform a full strain correction [10, 50]. Currently the only model [12] describing the modification of the diffusion tensor in response to strain assumes that the myocardium can be modelled as a homogeneous elastic medium. While it is clear that diffusion measured with a monopolar STEAM sequence over 2 cardiac cycles should be affected by cyclical strain, the complex multi-scale structure of the heart means that the exact effects of strain are more complex than those described by the existing model. We have recently highlighted issues with the results provided by the model by comparing ex-vivo and in-vivo STEAM DT-CMR in pigs [13]. The correlation between E2A and peak radial strain could be due to the strain effect, but E2A mobility (systole-diastole) obtained using the strain insensitive M2-SE technique also correlates with peak radial strain ( $p = 0.01$ ). Furthermore, it is logical to expect a correlation between E2A mobility and radial strain even in the absence of the effects of strain on the DT-CMR acquisition. The change in sheetlet angle represents the primary mechanism behind wall thickening [1] and we have recently validated these changes in a pre-clinical model [6]. However, we do expect some contribution of strain to the E2A mobility measured with STEAM and this may be reflected in the correlation ( $p < 0.01$ ) of differences in E2A between sequences with strain in both diastole and systole. Recent work comparing arrested and beating heart measures of

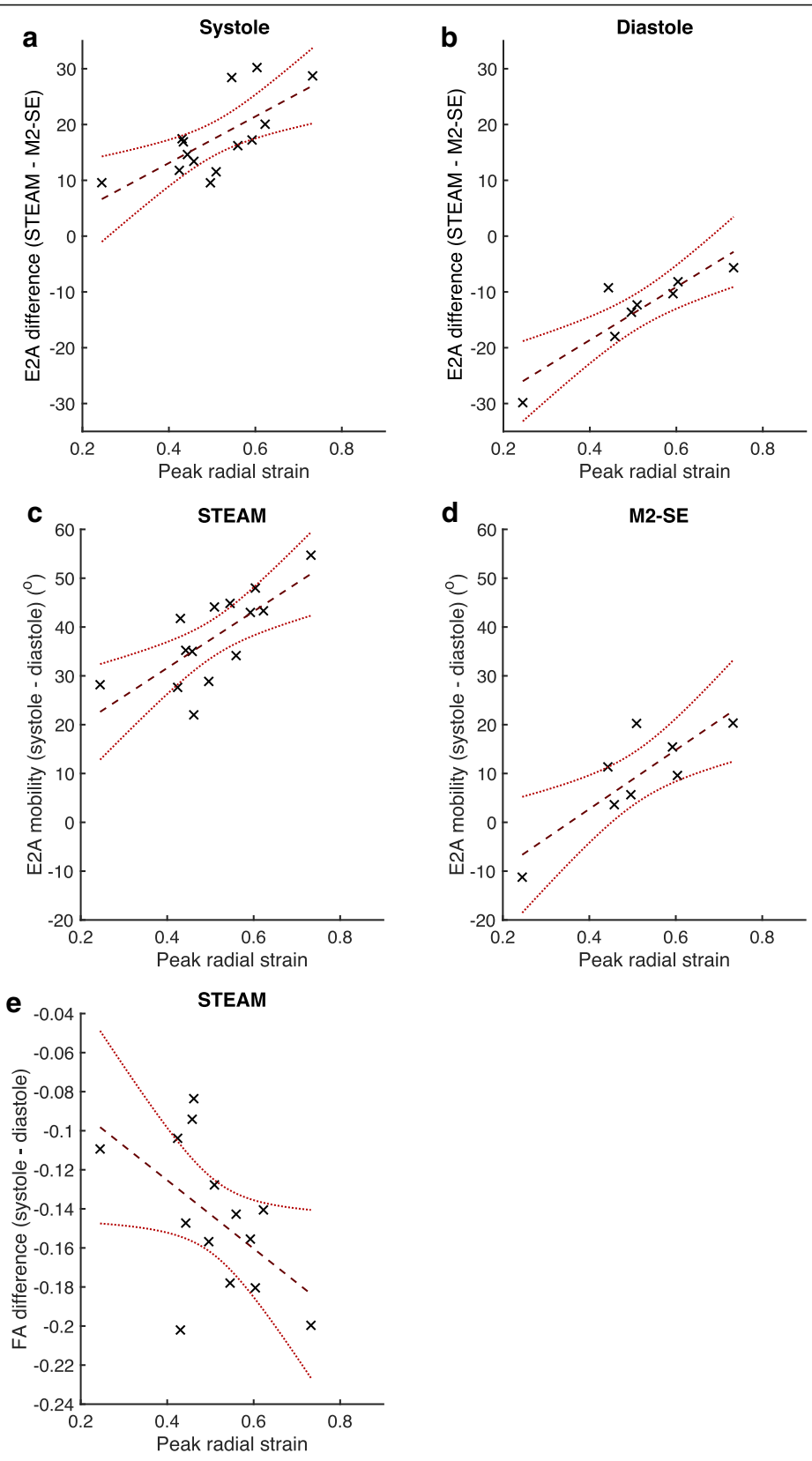


**Fig. 10** (See legend on next page.)

(See figure on previous page.)

**Fig. 10** Significant correlations with strain. Scatter plots and linear regressions for all significant ( $p < 0.05$ ) correlations between differences in DT-CMR parameters (between STEAM and M2-SE [a, b] or between systole and diastole [c-e]) and peak radial strain obtained from the 2D DENSE data. Linear regressions are shown as dashed lines and the 95% confidence intervals (functional non-simultaneous bounds) for the regression are shown in red dotted lines. Details of the fit parameters are given in Supporting Table S2

E2A in relaxed and contracted states, estimated the maximum component of E2A mobility attributable to strain [6] as  $\sim 17\%$ . The median E2A mobility measured in this study using STEAM of  $40^\circ$  compared to  $11^\circ$  measured with M2-SE (Supporting Table S1) suggests that strain is not the only contributor to this difference. A component of the difference between parameters other than E2A may also be the result of strain effects. While an ex-vivo study has demonstrated changes in eigenvalues and FA between contracted and relaxed states, MD was maintained [51]. As a result, we can estimate the maximum possible contribution of strain to MD measured with STEAM as the difference between the sweet-spot and the diastolic or systolic values. These differences of  $0.05 \times 10^{-3} \text{mm}^2 \cdot \text{s}^{-1}$  and  $0.06 \times 10^{-3} \text{mm}^2 \cdot \text{s}^{-1}$  (calculated from values in Supporting Table S1) at systole and diastole respectively, suggest that strain is not a major contributor to the much larger difference in MD observed between the two sequences. Indeed, even at the sweet-spot, where the existing model predicts minimal strain effects for STEAM data, there are large differences between the results from the two sequences.

The difference in diffusion time between these two sequences is expected to result in changes in the DT-CMR results [21, 52]. During the diffusion time of the STEAM sequence ( $\sim 1$  cardiac cycle,  $\sim 1000$  ms), free water molecules would diffuse a root mean square distance of around  $75 \mu\text{m}$  ( $D = 3 \times 10^{-3} \text{mm}^2 \cdot \text{s}^{-1}$  at  $37^\circ \text{C}$  [41]), while the equivalent distance for the M2-SE sequence (diffusion time  $\sim 20$  ms) is only around  $10 \mu\text{m}$ , which is less than typical cardiomyocyte dimensions (see Fig. 11). This limits the number of diffusing water molecules interacting with cellular structures and, while meaningful theoretical predictions of the strength of this effect are impossible without complex numerical simulations, previous work in ex-vivo tissue can provide some insights. Kim et al. [52] studied the diffusion time dependence in fresh samples of calf heart. Increasing the diffusion time from 33 ms to 412 ms resulted in an increase of FA from  $0.40 \pm 0.07$  to  $0.59 \pm 0.06$  and a reduction in MD from  $1.59 \pm 0.12 \times 10^{-3} \text{mm}^2 \cdot \text{s}^{-1}$  to  $1.33 \pm 0.08 \times 10^{-3} \text{mm}^2 \cdot \text{s}^{-1}$ . Despite the obvious limitations of comparing with ex-vivo tissue, these results suggest that the changes we observe here between sequences are predominantly a consequence of diffusion time effects. A recent review by Kiselev [53] suggests that probing cellular muscle structure is only possible with the longer diffusion times available with stimulated echoes and we might expect reductions in the uncertainty of angular DT-CMR measures with such sequences.

A further consequence of using a full cardiac cycle as the diffusion time in the STEAM sequence is that the b-value is modulated by variations in the RR-interval. In order to account for this b-value variation we corrected the b-values used in the tensor reconstruction based on the time stamps of the DICOM images. However, the time dependence of the measured diffusion is not accounted for in this correction, but should be small for typical variations in the RR-interval (the mean of the intra-subject standard deviation of the RR-interval was 5 ms) [52].

Using phantom data we demonstrate a 1.75 factor increase in SNR per image using the M2-SE sequence over STEAM. Due to the longer T1 and shorter T2 of myocardial tissue, the theoretical SNR ratio is lower in vivo than in the phantom. Based on Eq. 1 the theoretical SNR ratio in vivo is  $\text{SNR}_{\text{SE}}/\text{SNR}_{\text{STEAM}} = 1.37$ , assuming myocardial  $T_2 = 45 \pm 4$  ms (T2-prepared method [54], measured in 20 subjects in earlier work [24]),  $T_1 = 1327 \pm 59$  ms (modified Look Locker 5(3)3 [39, 40], in the same 20 subjects) and an RR interval of 970 ms. In the “b0” data we measured a median [interquartile range] in-vivo SNR ratio of  $\text{SNR}_{\text{SE}}/\text{SNR}_{\text{STEAM}}$  0.78 [0.38], 0.68 [0.23] and 0.59 [0.38] at systole, sweet-spot and diastole. These ratios are lower than the results of von Deuster et al. [21], who measured SNR efficiency and less than theoretically predicted. SNR per image measured using the multiple repetitions method is affected not only by true image noise but also by variations in signal intensity due to motion related signal loss,

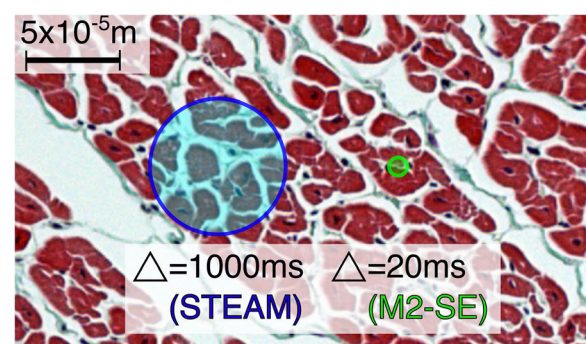


**Fig. 11** Distances diffused during the diffusion time. Comparison of the average distance diffused by water molecules during the diffusion time of the STEAM (blue circle) and M2-SE (green circle) sequences. The distances are super-imposed on a histology image cut from a pig heart perpendicular to the myocyte long axis. Based on a diffusivity of  $3 \times 10^{-3} \text{mm}^2 \cdot \text{s}^{-1}$ , free water molecules at  $37^\circ \text{C}$  would diffuse around  $75 \mu\text{m}$  during the diffusion time of the STEAM sequence, but only  $10 \mu\text{m}$  during the diffusion time of the M2-SE sequence



imperfect registration and residual blood signal. In this work, EPI readouts, receive gain, receive coils, reconstruction schemes and image scaling were matched between sequences and it is therefore reasonable to assume that image noise is similar (and we have confirmed this is so in phantom experiments, not included here). Therefore, we use the ratio between mean signal intensities in the two sequences as a surrogate for SNR ratio with fewer confounding effects than the multiple repetitions method. The median [interquartile range] signal ratios (M2-SE/STEAM) were 1.01[0.21], 0.96[0.12] and 1.19[0.34] at systole, sweet-spot and diastole; suggesting that a substantial fraction of the reduction in M2-SE SNR per image measured using the multiple repetitions method relative to theory is due to the confounding factors discussed above. The remaining difference between mean signal ratio and the theoretical SNR ratio could be a consequence of sequence differences in the in-plane excitation profiles. Small M2 gradients are used as crushers around the 180° pulse in the “b0” acquisition and higher order motion during these gradients may also contribute to the reduction in measured mean signal ratio relative to theory. In practice the SNR per unit acquisition time (as calculated by von Deuster et al. (21)) of the M2-SE sequence is boosted beyond that measured here by the additional averages that can be acquired due to its shorter TR compared to STEAM. However, STEAM allows much higher b-values to be used with little penalty in TE [33] and therefore a potential increase in diffusion contrast to noise relative to the M2-SE sequence.

Our more comprehensive findings differ from the smaller studies of both von Deuster et al. [21] and Stoeck et al. [20], who did not report any unsuccessful DT-CMR acquisitions. At the sweet-spot we found similar mean FA using both sequences and MD using STEAM, but higher MD values using M2-SE ( $1.69 \pm 0.15 \times 10^{-3} \text{mm}^2 \cdot \text{s}^{-1}$  vs.  $1.43 \pm 0.06 \times 10^{-3} \text{mm}^2 \cdot \text{s}^{-1}$  (21)). There were a number of key differences between our work and these previous studies. While we imaged at 3 T with a widely available gradient strength Stoeck et al. [20] and von Deuster et al. [21] used a high strength gradient system ( $80 \text{mT} \cdot \text{m}^{-1}$ ,  $100 \text{T} \cdot [\text{m} \cdot \text{s}]^{-1}$ ) at 1.5 T. We used parallel imaging to shorten the EPI readout and used optimal diffusion encoding directions for gradient performance to achieve a similar TE for M2-SE (76 ms vs. 73 ms (20) vs. 70 ms [21]) and a shorter STEAM TE (25 ms vs. 31 ms(21)). We imaged at three cardiac phases rather than only at the systolic sweet spot. We acquired data during multiple breath holds, as did von Deuster et al. [21], which we have found to be a more reliable method of acquiring STEAM data, although M2-SE acquisitions may be well suited to navigator gated free-breathing acquisitions [20, 21]. There is also the potential confounding issue of experience. While our group has ~6 years experience acquiring and processing

STEAM DT-CMR data and one experienced operator (ADS: 11 years CMR experience, 5 years DT-CMR experience, >40 subjects imaged with M2-SE) imaged all 15 subjects, M2-SE is a relatively new and evolving technique [55]. Therefore, we biased our study to the advantage of M2-SE acquisitions by selecting trigger times for all systolic and diastolic acquisitions based on the optimal timing for M2-SE acquisitions.

## Conclusions

Using a clinical 3 T scanner with standard gradients, both DT-CMR sequences perform equally well at the systolic pause and are successful in the majority of subjects. STEAM can also be used reliably in diastole, but 2nd order motion compensation of M2-SE did not appear to adequately cope with the low magnitude but complex trajectory of the motion at this cardiac phase. There were clear differences between the results obtained using each of these methods and only a few of these differences correlated with measures of strain. These differences are predominantly the result of the 2 orders of magnitude difference in diffusion time between these two techniques. While M2-SE may be more suited to free-breathing studies or imaging subjects with arrhythmia, STEAM is a more robust acquisition when diastolic imaging is required. It is, therefore, vital to understand the differences between these two methods and obtain normal values for the sequence of choice when planning future patient studies.

## Additional file

**Additional file 1: Figures S1–S6 and Tables S1 and S2.** (PDF 3207 kb)

## Abbreviations

B: Diffusion weighting;  $b_{\text{main}}$ : Main diffusion weighting;  $b_{\text{ref}}$ : Reference diffusion weighting; DENSE: Displacement encoding with stimulated echoes; DT-CMR: Diffusion tensor cardiovascular magnetic resonance; E1, E2, E3: The first, second and third eigenvalues respectively; E2A: Absolute value of the second eigenvector angle; EPI: Echo planar imaging; FA: Fractional anisotropy; HA  $R^2$ : Pearson correlation coefficient of the linear regression of the helix angle with transmural depth; HA RMSE: Root mean square error of the linear regression of the helix angle with transmural depth; HA: Helix angle; HAG: Helical angle gradient; LV: Left ventricle/left ventricular; M2-SE: First and second order motion compensated spin-echo; MD: Mean diffusivity; PCA-TMIP: Principle component analysis – temporal maximum intensity projection; RF: Radiofrequency; ROI: Region-of-interest; SE: Spin echo; SENSE: Sensitivity encoding; SNR: Signal-to-noise ratio; STEAM: Stimulated echo acquisition mode; TA std.: Standard deviation of the transverse angle; TA: Transverse angle; TE: Echo time; TR: Repetition time

## Funding

Not applicable.

## Availability of data and materials

Raw DT-CMR images from this project will be made available on reasonable application to the authors.

## Authors' contributions

ADS Acquired data, processed data, developed CMR sequences and analysis tools, performed statistical analysis, designed the study, recruited subjects and

drafted the manuscript; SNV developed CMR sequences, assisted in drafting the manuscript and in study design; PFF developed DT-CMR analysis tools and assisted in drafting the manuscript; ZK assisted in study design and assisted in drafting the manuscript; PDG assisted in developing CMR sequences and assisted in drafting the manuscript; PK provided histology images and assisted in drafting the manuscript; DJP assisted in study design and in drafting the manuscript; DNF: designed the study and assisted in drafting the manuscript. All authors participated in critical revision of the manuscript and approved the final version.

#### Ethics approval and consent to participate

All subjects provided informed consent and the study was approved by National Research Ethics Service Committee London East, reference 10/H0701/112.

#### Consent for publication

Subjects provided consent for publication.

#### Competing interests

Professor Pennell is a consultant to Siemens and a stockholder and director of Cardiovascular Imaging Solutions. The remaining authors have no competing interests.

#### Publisher's Note

Springer Nature remains neutral with regard to jurisdictional claims in published maps and institutional affiliations.

#### Author details

<sup>1</sup>Cardiovascular Magnetic Resonance Unit, Royal Brompton and Harefield NHS Foundation Trust and Imperial College London, Sydney Street, London, UK. <sup>2</sup>National Heart and Lung Institute, Imperial College London, Sydney Street, London, UK. <sup>3</sup>National Heart Lung and Blood Institute, National Institutes of Health, Bethesda, MD, USA.

Received: 15 August 2017 Accepted: 18 December 2017

Published online: 03 January 2018

#### References

- Ferreira PF, Kilner PJ, McGill L-A, NIELLES-VALLESPIN S, Scott AD, Ho SY, McCarthy KP, Haba MM, Ismail TF, Gatehouse PD, et al. In vivo cardiovascular magnetic resonance diffusion tensor imaging shows evidence of abnormal myocardial laminar orientations and mobility in hypertrophic cardiomyopathy. *J Cardiovasc Magn Reson*. 2014;16:87.
- Nguyen C, Fan Z, Xie Y, Dawkins J, Tseliou E, Bi X, Sharif B, Dharmakumar R, Marbán E, Li D. In vivo contrast free chronic myocardial infarction characterization using diffusion-weighted cardiovascular magnetic resonance. *J Cardiovasc Magn Reson*. 2014;16:68.
- Sosnovik DE, Mekkaoui C, Huang S, Chen HH, Dai G, Stoeck CT, Ngoy S, Guan J, Wang R, Kostis WJ, et al. Microstructural impact of ischemia and bone marrow-derived cell therapy revealed with diffusion tensor magnetic resonance imaging tractography of the heart in vivo. *Circulation*. 2014;129(17):1731–41.
- Nguyen C, Lu M, Fan Z, Bi X, Kellman P, Zhao S, Li D. Contrast-free detection of myocardial fibrosis in hypertrophic cardiomyopathy patients with diffusion-weighted cardiovascular magnetic resonance. *J Cardiovasc Magn Reson*. 2015;17:107.
- Nguyen C, Fan Z, Xie Y, Pang J, Speier P, Bi X, Kobashigawa J, Li D. In vivo diffusion-tensor MRI of the human heart on a 3 tesla clinical scanner: an optimized second order (M2) motion compensated diffusion-preparation approach. *Magn Reson Med*. 2016;76(5):1354–63.
- NIELLES-VALLESPIN S, Khalique Z, Ferreira PF, de Silva R, Scott AD, Kilner P, McGill L-A, Giannakidis A, Gatehouse PD, Ennis D, et al. Assessment of myocardial microstructural dynamics by in vivo diffusion tensor cardiac magnetic resonance. *J Am Coll Cardiol*. 2017;69(6):661–76.
- von Deuster C, Sammut E, Asner L, Nordsletten D, Lamata P, Stoeck CT, Kozerke S, Razavi R. Studying Dynamic Myofiber Aggregate Reorientation in Dilated Cardiomyopathy Using In Vivo Magnetic Resonance Diffusion Tensor Imaging. *Circulation: Cardiovascular Imaging*. 2016;9(10):e005018.
- Edelman RR, Gaa J, Wedeen VJ, Loh E, Hare JM, Prasad P, Li W. In vivo measurement of water diffusion in the human heart. *Magn Reson Med*. 1994;32(3):423–8.
- NIELLES-VALLESPIN S, Mekkaoui C, Gatehouse P, Reese TG, Keegan J, Ferreira PF, Collins S, Speier P, Feiweier T, de Silva R, et al. In vivo diffusion tensor MRI of the human heart: reproducibility of breath-hold and navigator-based approaches. *Magn Reson Med*. 2013;70(2):454–65.
- Stoeck CT, Kalinowska A, von Deuster C, Harmer J, Chan RW, Niemann M, Manka R, Atkinson D, Sosnovik DE, Mekkaoui C, et al. Dual-phase cardiac diffusion tensor imaging with strain correction. *PLoS One*. 2014;9(9):e107159.
- Ferreira P, Kilner PJ, McGill L-A, NIELLES-VALLESPIN S, Scott AD, Spottiswoode BS, Zhong X, Ho SY, McCarthy KP, Ismail TF, et al. Aberrant myocardial sheetlet mobility in hypertrophic cardiomyopathy detected using in vivo cardiovascular magnetic resonance diffusion tensor imaging. *J Cardiovasc Magn Reson*. 2014;16(suppl 1):338.
- Reese W. Weisskoff. Measuring diffusion in the presence of material strain. *J Magn Reson B*. 1996;112(3):253–8.
- Ferreira PF, NIELLES-VALLESPIN S, Scott AD, de Silva R, Kilner PJ, Ennis DB, Auger DA, Suever JD, Zhong X, Spottiswoode BS, et al. Evaluation of the impact of strain correction on the orientation of cardiac diffusion tensors with in vivo and ex vivo porcine hearts. *Magnetic Resonance in Medicine*. 2017. Epub ahead of print. doi: <https://doi.org/10.1002/mrm.26850>.
- Tseng WY, Reese TG, Weisskoff RM, Wedeen VJ. Cardiac diffusion tensor MRI in vivo without strain correction. *Magn Reson Med*. 1999;42(2):393–403.
- Le Bihan D, Johansen-Berg H. Diffusion MRI at 25: exploring brain tissue structure and function. *NeuroImage*. 2012;61(2):324–41.
- Horsfield MA, Jones DK. Applications of diffusion-weighted and diffusion tensor MRI to white matter diseases - a review. *NMR Biomed*. 2002;15(7–8):570–7.
- Gamper U, Boesiger P, Kozerke S. Diffusion imaging of the in vivo heart using spin echoes—considerations on bulk motion sensitivity. *Magn Reson Med*. 2007;57(2):331–7.
- Welsh CL, DiBella EVR, Hsu EW. Higher-order motion-compensation for in vivo cardiac diffusion tensor imaging in rats. *IEEE Trans Med Imaging*. 2015;34(9):1843–53.
- Nguyen C, Fan Z, Sharif B, He Y, Dharmakumar R, Berman DS, Li D. In vivo three-dimensional high resolution cardiac diffusion-weighted MRI: a motion compensated diffusion-prepared balanced steady-state free precession approach. *Magn Reson Med*. 2014;72(5):1257–67.
- Stoeck CT, von Deuster C, Genet M, Atkinson D, Kozerke S. Second-order motion-compensated spin Echo diffusion tensor imaging of the human heart. *Magn Reson Med*. 2015;75(4):1669–76.
- von Deuster C, Stoeck CT, Genet M, Atkinson D, Kozerke S. Spin echo versus stimulated echo diffusion tensor imaging of the in vivo human heart. *Magn Reson Med*. 2016;76(3):862–72.
- Feinberg DA, Turner R, Jakab PD, Von Kienlin M. Echo-planar imaging with asymmetric gradient modulation and inner-volume excitation. *Magn Reson Med*. 1990;13(1):162–9.
- Pruessmann KP, Weiger M, Scheidegger MB, Boesiger P. SENSE: sensitivity encoding for fast MRI. *Magn Reson Med*. 1999;42(5):952–62.
- Scott AD, NIELLES-VALLESPIN S, Ferreira PF, Gatehouse PD, Khalique Z, Kilner PJ, Pennell DJ, Firmin DN. A comparison of M012 compensated spin-echo and STEAM cardiac DTI at multiple cardiac phases. In Proceedings: International Society for Magnetic Resonance in Medicine Annual Meeting. 2016:3115.
- Scott AD, Ferreira PFADC, NIELLES-VALLESPIN S, Gatehouse P, McGill L-A, Kilner P, Pennell DJ, Firmin DN. Optimal diffusion weighting for in vivo cardiac diffusion tensor imaging. *Magn Reson Med*. 2014;74(2):420–30.
- Reeder SB, Wintersperger BJ, Dietrich O, Lanz T, Greiser A, Reiser MF, Glazer GM, Schoenberg SO. Practical approaches to the evaluation of signal-to-noise ratio performance with parallel imaging: application with cardiac imaging and a 32-channel cardiac coil. *Magn Reson Med*. 2005;54(3):748–54.
- Scott AD, Ferreira PF, NIELLES-VALLESPIN S, Pennell DJ, Firmin DN. Can we predict the diffusion “sweet-spot” based on a standard cine? *J Cardiovasc Magn Reson*. 2016;18(Suppl 1):W17.
- Aletras AH, Ding S, Balaban RS, Wen H. DENSE: displacement encoding with stimulated echoes in cardiac functional MRI. *J Magn Reson*. 1999;137(1):247–52.
- Zhong X, Spottiswoode BS, Meyer CH, Kramer CM, Epstein FH. Imaging three-dimensional myocardial mechanics using navigator-gated volumetric spiral cine DENSE MRI. *Magn Reson Med*. 2010;64(4):1089–97.
- Scott AD, Tayal U, NIELLES-VALLESPIN S, Ferreira P, Zhong X, Epstein FH, Prasad SK, Firmin D. Accelerating cine DENSE using a zonal excitation. *J Cardiovasc Magn Reson*. 2016;18(Suppl 1):O50.

31. Zhong X, Spottiswoode BS, Cowart EA, Gilson WD, Epstein FH. Selective suppression of artifact-generating echoes in cine DENSE using through-plane dephasing. *Magn. Reson. Med.* 2006;56(5):1126–31.
32. McGill L-A, Ismail TF, Nielles-Vallespin S, Ferreira P, Scott AD, Roughton M, Kilner PJ, Ho SY, McCarthy KP, Gatehouse PD, et al. Reproducibility of in-vivo diffusion tensor cardiovascular magnetic resonance in hypertrophic cardiomyopathy. *J Cardiovasc Magn Reson.* 2012;14:86.
33. Scott AD, Nielles-Vallespin S, Ferreira PF, McGill L-A, Pennell DJ, Firmin DN. The effects of noise in cardiac diffusion tensor imaging and the benefits of averaging complex data. *NMR Biomed.* 2016;29(5):588–99.
34. Ennis DB, Kindlmann G. Orthogonal tensor invariants and the analysis of diffusion tensor magnetic resonance images. *Magn Reson Med.* 2006;55(1):136–46.
35. McGill LA, Ferreira PF, Scott AD, Nielles-Vallespin S, Giannakidis A, Kilner PJ, Gatehouse PD, de Silva R, Firmin DN, Pennell DJ. Relationship between cardiac diffusion tensor imaging parameters and anthropometrics in healthy volunteers. *J Cardiovasc Magn Reson.* 2016;18(1):2.
36. Lombaert H, Peyrat J-M, Croisille P, Rapacchi S, Fanton L, Cheriet F, Clarysse P, Magnin I, Delingette H, Ayache N. Human atlas of the cardiac fiber architecture: study on a healthy population. *IEEE Trans Med Imaging.* 2012;31(7):1436–47.
37. Spottiswoode BS, Zhong X, Hess AT, Kramer CM, Meintjes EM, Mayosi BM, Epstein FH. Tracking myocardial motion from cine DENSE images using spatiotemporal phase unwrapping and temporal fitting. *IEEE Trans Med Imaging.* 2007;26(1):15–30.
38. Gilliam A, Suever J, Contributors. DENSEanalysis. Retrieved from <https://github.com/denseanalysis/denseanalysis>. 2016.
39. Kellman P, Wilson JR, Xue H, Ugander M, Arai AE. Extracellular volume fraction mapping in the myocardium, part 1: evaluation of an automated method. *J Cardiovasc Magn Reson.* 2012;14:63.
40. Messroghli DR, Radjenovic A, Kozerke S, Higgins DM, Sivananthan MU, Ridgway JP. Modified look-locker inversion recovery (MOLLI) for high-resolution T1 mapping of the heart. *Magn Reson Med.* 2004;52(1):141–6.
41. Mills R. Self-diffusion in normal and heavy water in the range 1–45°C. *J Phys Chem.* 1973;77(5):685–8.
42. Stoock CT, von Deuster C, Kozerke S. Second-order motion-compensated spin echo diffusion tensor imaging of the in vivo human heart – considerations on gradient performance requirements. In Proceedings: International Society for Magnetic Resonance in Medicine Annual Meeting. 2016:3114.
43. Stoock CT, von Deuster C, van Gorkum R, Kozerke S. Impact of eddy-currents and cardiac motion in DTI of the in-vivo heart - a comparison of second-order motion compensated SE versus STEAM. In Proceedings: International Society for Magnetic Resonance in Medicine Annual Meeting. 2017:926.
44. Mekkaoui I, Moulin K, Croisille P, Pousin J, Viallon M. Quantifying the effect of tissue deformation on diffusion-weighted MRI: a mathematical model and an efficient simulation framework applied to cardiac diffusion imaging. *Phys Med Biol.* 2016;61(15):5662–86.
45. Simpson R, Keegan J, Firmin D. Efficient and reproducible high resolution spiral myocardial phase velocity mapping of the entire cardiac cycle. *J Cardiovasc Magn Reson.* 2013;15(1):34.
46. Froeling M, Strijkers GJ, Nederveen AJ, Luijten PR. Whole heart DTI using asymmetric bipolar diffusion gradients. *J Cardiovasc Magn Reson.* 2015;17(1):P15.
47. Pai VM, Rapacchi S, Kellman P, Croisille P, Wen H. PCATMIP: enhancing signal intensity in diffusion-weighted magnetic resonance imaging. *Magn Reson Med.* 2011;65(6):1611–9.
48. Wei H, Viallon M, Delattre BMA, Moulin K, Yang F, Croisille P, Zhu Y. Free-breathing diffusion tensor imaging and Tractography of the human heart in healthy volunteers using wavelet-based image fusion. *IEEE Trans Med Imaging.* 2015;34(1):306–16.
49. Pannu HK, Alvarez W, Fishman EK.  $\beta$ -Blockers for Cardiac CT: A Primer for the Radiologist. *Am. J. Roentgenol.* 2006;186(6 supplement 2):S341–5.
50. Reese TG, Weisskoff RM, Smith RN, Rosen BR, Dinsmore RE, Wedeen VJ. Imaging myocardial fiber architecture in vivo with magnetic resonance. *Magn Reson Med.* 1995;34(6):786–91.
51. Nielles-Vallespin S, Ferreira PF, Scott AD, de Silva R, Kilner PJ, Ennis DB, Pennell DJ, Firmin DN, Arai AE. Characterisation of in-vivo and ex-vivo cardiac diffusion tensor imaging scalar measures of cardiac microstructure in healthy swine. In Proceedings: International Society for Magnetic Resonance in Medicine Annual Meeting 2017:929.
52. Kim S, Chi-Fishman G, Barnett AS, Pierpaoli C. Dependence on diffusion time of apparent diffusion tensor of ex vivo calf tongue and heart. *Magn Reson Med.* 2005;54(6):1387–96.
53. Kiselev VG. Fundamentals of diffusion MRI physics. *NMR Biomed.* 2017;30(3):e3602.
54. Giri S, Chung Y-C, Merchant A, Mihai G, Rajagopalan S, Raman SV, Simonetti OP. T2 quantification for improved detection of myocardial edema. *J Cardiovasc Magn Reson.* 2009;11:56.
55. Aliotta E, Wu HH, Ennis DB. Convex optimized diffusion encoding (CODE) gradient waveforms for minimum echo time and bulk motion-compensated diffusion-weighted MRI. *Magn Reson Med.* 2017;77(2):717–29.

Submit your next manuscript to BioMed Central and we will help you at every step:

- We accept pre-submission inquiries
- Our selector tool helps you to find the most relevant journal
- We provide round the clock customer support
- Convenient online submission
- Thorough peer review
- Inclusion in PubMed and all major indexing services
- Maximum visibility for your research

Submit your manuscript at  
[www.biomedcentral.com/submit](http://www.biomedcentral.com/submit)

